Journal of Magnetic Resonance 302 (2019) 14–20

Contents lists available at ScienceDirect

Journal of Magnetic Resonance

journal homepage: www.elsevier.com/locate/jmr

"Radiation Damping" in gas spin comagnetometers

Zhiguo Wang [a,b,*], Xiang Peng [c], Rui Zhang [d], Hui Luo [a,b], Hong Guo [c]

[a] College of Advanced Interdisciplinary Studies, National University of Defense Technology, Changsha 410073, PR China
[b] Interdisciplinary Center of Quantum Information, National University of Defense Technology, Changsha 410073, PR China
[c] State Key Laboratory of Advanced Optical Communication Systems and Networks, School of Electronics Engineering and Computer Science, and Center for Quantum Information Technology, Peking University, Beijing 100871, PR China
[d] College of Liberal Arts and Sciences, National University of Defense Technology, Changsha 410073, PR China

ARTICLE INFO

Article history:
Received 27 November 2018
Revised 9 March 2019
Accepted 13 March 2019
Available online 15 March 2019

Keywords:
Spin comagnetometer
Radiation damping
Spin-exchange optical pumping

ABSTRACT

We report a new kind of interaction between overlapping Rb-Xe spin ensembles polarized by spin-exchange optical pumping. The Rb acts as both a medium to optically polarize the Xe spins and as a magnetometer to probe the precession of Xe spins. When Xe spins precess, they result in the precession of Rb spins. Like the radiation damping effect caused by the coil in conventional NMR systems, the precessing Rb spins lead to damping and a frequency-shift for the precessing Xe spins. When Xe spins are operated in a free-induction decay mode, the transverse relaxation time and oscillating frequency of Xe spins change due to the "radiation damping" effect of Rb spins. When Xe spins are operated in the self-oscillating mode, its transverse relaxation time and oscillating frequency will also be changed. These effects will influence the accuracy of NMR probes, which are widely used in the search for CPT- and Lorentz-invariance violations, the fifth force, etc. If this problem is solved or compensated for, the limit of the aforementioned search may be improved.

1. Introduction

New physics beyond the standard model has attracted wide interest, such as T-odd and P-odd interactions from axion-like particles as well as Lorentz-invariance and CPT-violating effects [1–8]. Scientists have proposed many methods to detect them, in which probes with spins are very promising for their unique interactions with posited background fields and high sensitivity [1–8]. Various parameters of spin ensembles can be used to detect these interactions, including the precession frequency [3], longitudinal relaxation time and transverse relaxation time [7,8]. When the precession frequency is used, the spins can be operated in either the free-precession or self-oscillation mode. Both modes suffer from a precession frequency shift, and the main cause of such a frequency shift is the fluctuation of bias (longitudinal static) magnetic field. A comagnetometer is an efficient way to solve this problem, such as a ^{3}He-^{129}Xe comagnetometer [1], a Rb-^{129}Xe-^{131}Xe comagnetometer [3], or a K-^{3}He comagnetometer [9]. However, the spin interactions between different species also produce frequency shifts that cannot be neglected, such as a longitudinal magnetic field from spin magnetization [10] or a Ramsey-Bloch-Siegert shift (RBS shift) [11]. Moreover, there are also some types of frequency shifts that cannot be common-mode suppressed, such as the electronic quadrupolar effect in the Rb-^{129}Xe-^{131}Xe comagnetometer [3] and the second order magnetic gradient effect [12].

In some comagnetometers made of alkali vapor and noble gas, such as the Rb-^{129}Xe-^{131}Xe comagnetometer, both the built-in magnetometer made of alkali spins [3,11] and the induction coil [13] can be used to extract the nuclear magnetic resonance (NMR) signal of the noble gas. In the latter case, it is well known that the induction coil gives back action to the precessing spins by the so-called radiation damping effect, which leads to damping and frequency shift of the nuclear spins [14–16]. However, the back action from the built-in magnetometer made of alkali spins, as far as we know, has not attracted much attention. Taking the Rb-^{129}Xe comagnetometer as an example, we analyzed the effect of the back action of Rb spins on the motion of ^{129}Xe nuclear spins. We find that, as do the induction coils in NMR systems, the Rb spins give back action to the precessing nuclear spins. The main consequence of the back action is the damping and frequency shift of the precessing nuclear spins. This phenomenon is similar to the radiation damping effect caused by the induction coil in conventional NMR experiments, and thus, we might as well call it the "radiation damping" effect. Therefore, this kind of back action should be paid attention to in order to improve the measurement precision using a precessing frequency and/or transverse

* Corresponding author at: College of Advanced Interdisciplinary Studies, National University of Defense Technology, Changsha 410073, PR China.
E-mail address: maxborn@nudt.edu.cn (Z. Wang).

https://doi.org/10.1016/j.jmr.2019.03.004
1090-7807/

relaxation time in comagnetometers. In this paper, we find that the back action can be reduced through using a larger static magnetic field for those comagnetometers using the precessing frequency to detect physical parameters.

2. Theoretical analysis

Considering the Rb-Xe system in Fig. 1 [11,17], a glass cell contains some amounts of N_2, He, and ^{129}Xe as well as a droplet of Rb, which will be vaporized when heated to approximately 100 °C. Both the Rb spins and Xe spins are polarized with the spin-exchange-optical-pumping technique [18]. When a static magnetic field B_0 is applied along the z-axis, the Rb spins act as a magnetometer that is sensitive to the magnetic field in the xy plane [17].

Due to the Fermi-contact between Rb electrons and Xe nuclei, the nuclear spins and electronic spins are coupled through spin-exchange and interact based on the average magnetization of the other [10]. The coupled Bloch equations for Xe and Rb magnetizations are as follows:

$$\begin{aligned}\frac{\partial \boldsymbol{M}^e}{\partial t} &= \frac{\gamma_e'}{S(\beta)}(\boldsymbol{B}+\lambda\boldsymbol{M}^n)\times\boldsymbol{M}^e + \frac{M_0^e\hat{z}-\boldsymbol{M}^e}{\{T_2'^e,T_2'^e,T_1'^e\}S(\beta)}\\ \frac{\partial \boldsymbol{M}^n}{\partial t} &= \gamma_n(\boldsymbol{B}+\lambda\boldsymbol{M}^e)\times\boldsymbol{M}^n + \frac{M_0^n\hat{z}-\boldsymbol{M}^n}{\{T_2^n,T_2^n,T_1^n\}}\end{aligned}, \tag{1}$$

where $\boldsymbol{M}^e$ and $\boldsymbol{M}^n$ are the magnetization vectors of Rb electrons and Xe nuclei, respectively, γ_e' and γ_n are the gyromagnetic ratios of the electronic spin and Xe nuclear spin, respectively, and $S(\beta)$ is the "slowing-down factor" due to the sharing of the angular momentum between the Rb electron and Xe nuclear spins, which depends on electron spin temperature β. $\boldsymbol{B}$ is the total magnetic field vector that is applied externally, λ is a coefficient that represents the interaction strength between Rb and Xe atoms, $\boldsymbol{M}_0^e$ and $\boldsymbol{M}_0^n$ are the equilibrium magnetizations of Rb and Xe, respectively, and $T_2'^e$, $T_1'^e$, T_2^n, and T_1^n are the transverse and longitudinal relaxation times of the electronic spin and Xe nuclear spin, respectively. The $\{T_2'^e, T_2'^e, T_1'^e\}$ and $\{T_2^n, T_2^n, T_1^n\}$ mean that we should use the relaxation time with a subscript "2" for the differential equation of x and y components of the magnetization and that with a subscript "1" for the differential equation of the z component.

The dynamics of two overlapping spin ensembles interacting by spin-exchange depends on the parameters of the spin system. The dynamics when the nuclear and electronic spin precession frequencies are nearly matched at very low magnetic field strengths have been analyzed in [10,19], where the interactions of the nuclear and electronic spins are very strong. Here, we are interested in another condition in which the applied magnetic field $\boldsymbol{B}$ is of the order of μT and much larger than the magnetic field produced by the magnetization of spins, making the interactions of the nuclear and electronic spins very weak. Therefore, the coupled Bloch equations can be solved with the perturbation-iteration method. Since the magnetization field is much less than the applied magnetic field, the independent Bloch equations can be seen as the zeroth order solution. Both the nuclear and electronic spin move in accordance with the Bloch equations. The flow chart of the perturbation-iteration method is shown in Fig. 2.

For the coupled system shown in Fig. 1, Rb and Xe are polarized along the z-axis. Since we assume the coupling is weak, we can reduce Eq. (1) to the following two Bloch equations:

$$\frac{d\boldsymbol{M}^e}{dt} = \gamma_e(\boldsymbol{B}+\lambda M_0^n\hat{z})\times\boldsymbol{M}^e + \frac{M_0^e\hat{z}-\boldsymbol{M}^e}{\{T_2^e,T_2^e,T_1^e\}}, \tag{2}$$

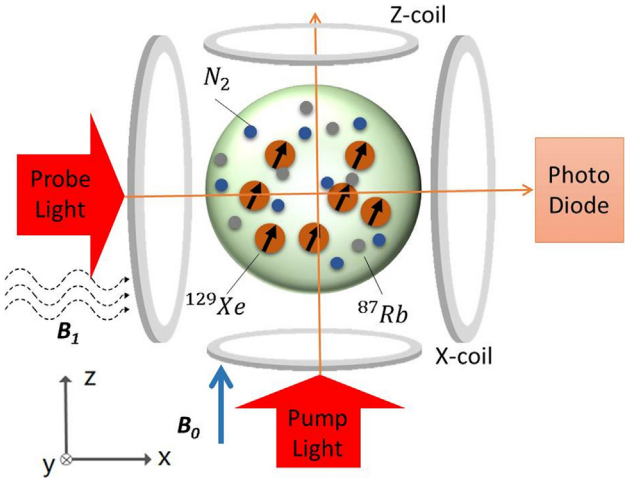

Fig. 1. A typical Rb-Xe comagnetometer. The Rb spins are polarized with the left circularly polarized laser beam, and the Xe nuclear spins are polarized with spin-exchange between the Rb spins. When a static magnetic field B_0 is applied along the z-axis, both the Rb and Xe nuclear spins can precess about the z-axis. A probe light propagating along the x-axis detects the x component of Rb magnetization, which reflects the magnetic field in the xy plane. The nuclear spins can be manipulated by oscillating the magnetic field in the x direction. Depending on the manipulation mode for the magnetic field, the nuclear spins can be in a free-precession or self-oscillation state. The oscillating magnetic field in the x direction changes the state of Rb spins, and meanwhile, a back action can be exerted on Xe spins.

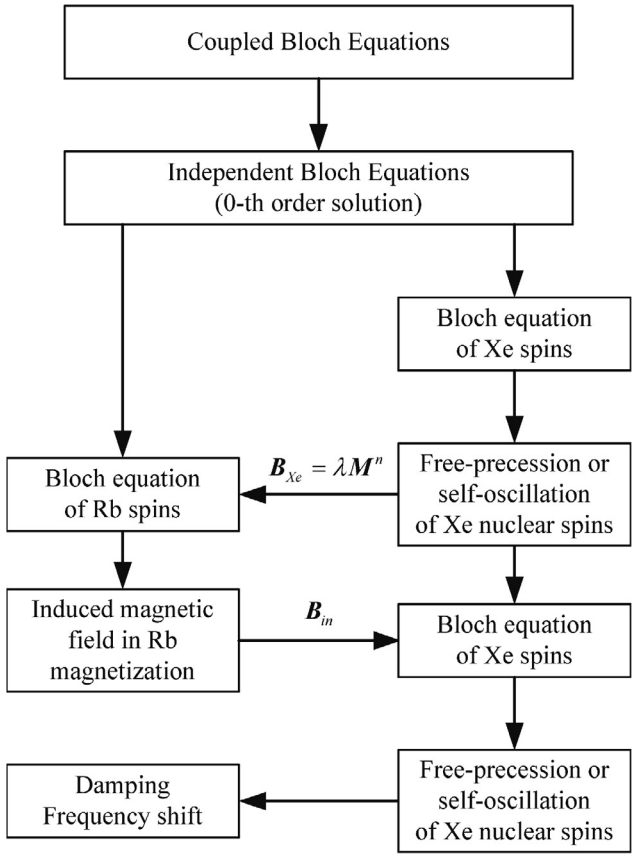

Fig. 2. Flow chart of the perturbation-iteration method. In the 0-th order solution, the Bloch equations for electrons and nuclei are solved independently. Depending on the configuration of the Rb-Xe comagnetometer, we can obtain the free-precession or self-oscillation solution from the Bloch equation of Xe spins. To be specific, the nuclear spins precess about the z-axis, which produce a precessing magnetic field. The precession of Xe spins affects the Bloch equation of Rb spins as an effective magnetic field. Then, the Rb spins produce an effective magnetic field, which affects the Bloch equation of Xe spins. As a result, the precessing Rb magnetization causes damping and frequency shift effects for the precessing Xe spins.

$$\frac{d\boldsymbol{M}^n}{dt}=\gamma_n(\boldsymbol{B}+\lambda M_0^e\hat{z})\times\boldsymbol{M}^n+\frac{M_0^n\hat{z}-\boldsymbol{M}^n}{\{T_2^n,T_2^n,T_1^n\}},\tag{3}$$

where M_0^e and M_0^n are the equilibrium magnetizations of electronic and nuclear spins, respectively, $\gamma_e=\frac{\gamma_e'}{S(\beta)}$, $T_2^e=S(\beta)T_2'^e$, and $T_1^e=S(\beta)T_1'^e$.

First, we analyze the dynamics of the Rb spin from Eq. (2),

$$\frac{d\boldsymbol{M}^e}{dt}=\gamma_e\tilde{\boldsymbol{B}}\times\boldsymbol{M}^e-\left(\frac{M_x^e}{T_2^e}\hat{x}+\frac{M_y^e}{T_2^e}\hat{y}-\frac{M_0^e\hat{z}-M_z^e}{T_1^e}\right),\tag{4}$$

where the magnetic field sensed by Rb spins is as follows:

$$\tilde{\boldsymbol{B}}=\left\{\tilde{B}_x,\tilde{B}_y,B_0+\lambda M_0^n\right\}^T.\tag{5}$$

If we let $M_+^e=M_x^e+iM_y^e$, from Eq. (4) we obtain

$$\frac{d}{dt}M_+^e+\left(\frac{1}{T_2^e}-i\omega_0^e\right)M_+^e=-i\gamma_eM_z^e\left(\tilde{B}_x+i\tilde{B}_y\right)\tag{6}$$

and

$$\frac{d}{dt}M_z^e+\frac{1}{T_1^e}M_z^e=\frac{1}{T_1^e}M_0^e-\gamma_e\left(M_x^e\tilde{B}_y-M_y^e\tilde{B}_x\right)\tag{7}$$

where $\omega_0^e=\gamma_e(B_0+\lambda M_0^n)$.

Since the applied transverse magnetic field B_x and the magnetic field produced by the magnetization of nuclei are very weak compared to B_0, the transverse magnetization components of electron spins M_x^e and M_y^e are very small. Therefore, from Eq. (7) we can obtain an approximate solution as follows:

$$M_z^e=M_0^e\tag{8}$$

Inserting Eq. (8) into Eq. (6), we know the transverse magnetization component M_+^e of Rb spins can be used to detect a weak magnetic field. From another angle, the motion of Rb spins will be changed by the weak magnetic field.

We are interested in the transverse rotating states of Xe spins in either the free induction decay (FID) or self-oscillation mode. The magnetization of nuclear spins can be described with the following equation:

$$\boldsymbol{M}^n=\{M_\perp^n\cos(\omega_0^nt+\psi),M_\perp^n\sin(\omega_0^nt+\psi),M_0^n\}^T,\tag{9}$$

where $M_\perp^n$ is the amplitude of transverse rotation and can be time-dependent or time independent, ω_0^n is the oscillating frequency, t is the time, and ψ is the phase. Then, the magnetic field sensed by the Rb spin will be as follows:

$$B^e=\begin{bmatrix}B_x\sin(\omega_0^nt)+\lambda M_\perp^n\cos(\omega_0^nt+\psi)\\ \lambda M_\perp^n\sin(\omega_0^nt+\psi)\\ B_0+\lambda M_z^n\end{bmatrix}=\left\{\tilde{B}_x,\tilde{B}_y,\tilde{B}_0\right\}^T.\tag{10}$$

The transverse magnetic field is as follows:

$$\tilde{B}_x+i\tilde{B}_y=B_x\sin(\omega_0^nt)+\lambda M_\perp^ne^{i\left(\omega_0^nt+\psi\right)}.\tag{11}$$

Substituting Eq. (11) into Eq. (6) and using the fact that ω_0^n is much less than ω_0^e, we can obtain

$$\begin{aligned}M_+^e&=-\frac{i\gamma_eT_2^eM_0^e\left(\tilde{B}_x+i\tilde{B}_y\right)}{(1+i\omega_0^eT_2^e)}\\&=-\frac{i\gamma_eT_2^eM_0^e\left[B_x\sin(\omega_0^nt)+\lambda M_\perp^ne^{i\left(\omega_0^nt+\psi\right)}\right]}{(1+i\omega_0^eT_2^e)}.\end{aligned}\tag{12}$$

This condition $\omega_0^n<<\omega_0^e$ is always true in our case since ω_0^n is the Larmor frequency of the nuclear spin and ω_0^e is the Larmor frequency of the electronic spin.

From Eq. (12), we know the Rb spins will precess with a frequency ω_0^n, producing a magnetic field which exerts an effect on nuclear spins and then changes their motion. We might as well take the magnetic field λM_+^e as the induction field, similar to the induction field in the coil of the conventional NMR system.

Similar to the derivations from Eqs. (4)–(7), the motion of nuclear spins can be described by

$$\frac{d}{dt}M_+^n+\left(\frac{1}{T_2^n}-i\omega_0^n\right)M_+^n=-i\gamma_nM_z^n\left(\tilde{B}_x^n+i\tilde{B}_y^n\right)\tag{13}$$

and

$$\frac{d}{dt}M_z^n+\frac{1}{T_1^n}M_z^n=\frac{1}{T_1^n}M_0^n-\gamma_n\left(M_x^n\tilde{B}_y^n-M_y^n\tilde{B}_x^n\right).\tag{14}$$

The magnetic fields sensed by nuclear spins are

$$\tilde{B}_x^n=B_x\sin(\omega_0^nt)+\lambda(M_+^e)_x\tag{15}$$

and

$$\tilde{B}_y^n=\lambda(M_+^e)_y,\tag{16}$$

where $(M_+^e)_x$ and $(M_+^e)_y$ are the x and y components of M_+^e, respectively.

For nuclear spins, the 0-th order Bloch equation is as follows:

$$\frac{d}{dt}M_\perp^n+\left(\frac{1}{T_2^n}-i\omega_0^n\right)M_\perp^n=-i\gamma_nM_z^nB_x\sin(\omega_0^nt),\tag{17}$$

that is, nuclear spins are precessing under the applied field $B_x\sin(\omega_0^nt)$, with a frequency ω_0^n and amplitude $M_\perp^n$. When considering the induction magnetic field from Rb spins, the frequency ω_0^n and amplitude $M_\perp^n$ may change accordingly. From Eq. (12), we know the induced magnetic field from Rb spins is as follows:

$$\begin{aligned}B_{in}^e=&-\frac{\gamma_eT_2^e(\lambda M_0^e)(i+\omega_0^eT_2^e)}{1+(\omega_0^eT_2^e)^2}\left[B_x\sin(\omega_0^nt)\right]\\&-\frac{\gamma_eT_2^e(\lambda M_0^e)(i+\omega_0^eT_2^e)}{1+(\omega_0^eT_2^e)^2}\left[\lambda M_\perp^ne^{i(\omega_0^nt+\psi)}\right].\end{aligned}\tag{18}$$

It is obvious that the induced magnetic field contains two origins. One is due to the applied magnetic field $B_x\sin(\omega_0^nt)$ and the other is due to the motion of Xe magnetization $M_\perp^n$.

By letting the nuclear spins oscillate with the frequency ω^n after considering the influence of Rb spins, we can write $M_x^n+iM_y^n=M_\perp^ne^{i\omega^nt+i\psi}$. According to Euler's formula, we know $\sin(\omega_0^nt)=\frac{1}{2i}(e^{i\omega^nt}-e^{-i\omega^nt})$. Under the rotation wave approximation, we have $\sin(\omega_0^nt)=\frac{1}{2i}e^{i\omega^nt}$. Then, Eq. (13) can be changed into

$$\frac{d}{dt}M_\perp^n=-i\Delta\omega^nM_\perp^n-\frac{M_\perp^n}{T_2^n}-\frac{\gamma_nM_z^nB_x}{2}e^{-i\psi}-i\gamma_nM_z^nB_{in}^ee^{-i\omega^nt-i\psi},\tag{19}$$

where $\Delta\omega^n=(\omega^n-\omega_0^n)$.

(1) In the FID mode, the resonant field $B_x\sin(\omega_0^nt)$ is turning off in the process of free-precession. Therefore, from Eq. (18) we have the following:

$$\begin{aligned}-i\gamma_nM_z^nB_{in}^ee^{-i\omega^nt-i\psi}=&-\frac{\gamma_n\gamma_eT_2^e(\lambda M_z^n)(\lambda M_0^e)}{1+(\omega_0^eT_2^e)^2}M_\perp^n+i\\&\times\frac{\gamma_n\gamma_eT_2^e(\lambda M_z^n)(\lambda M_0^e)(\omega_0^eT_2^e)}{1+(\omega_0^eT_2^e)^2}M_\perp^n.\end{aligned}\tag{20}$$

Substituting Eq. (20) into Eq. (19), we can easily find that the first term in Eq. (20) leads to the relaxation/damping of

$M_{\perp}^{n}$, while the second term leads to the frequency shift of the oscillator. The equivalent relaxation time caused by Rb spins is

$$\frac{1}{T_{eq}^{n}}=\frac{\gamma_n\gamma_e T_2^e(\lambda M_z^n)(\lambda M_0^e)}{1+(\omega_0^e T_2^e)^2}, \tag{21}$$

and the frequency shift is

$$\Delta\omega^n=-\frac{\gamma_n\gamma_e T_2^e(\lambda M_z^n)(\lambda M_0^e)}{1+(\omega_0^e T_2^e)^2}(\omega_0^e T_2^e). \tag{22}$$

(2) In the self-oscillation mode, the resonant field $B_x\sin(\omega_0^n t)$ should be applied continuously so the Rb spins also give back action to the driving field B_x. For ideal self-sustained spin oscillators, $\psi=0$. From Eq. (18) we have

$$\begin{aligned}-i\gamma_n M_z^n B_{in}^e e^{-i\omega^n t-i\psi}=&\frac{\gamma_e\gamma_n T_2^e(\lambda M_z^n M_0^e)}{2\left[1+(\omega_0^e T_2^e)^2\right]}\{\omega_0^e T_2^e+i\}B_x\\&-\frac{\gamma_n\gamma_e T_2^e(\lambda M_z^n)(\lambda M_0^e)}{1+(\omega_0^e T_2^e)^2}M_{\perp}^n\\&+i\frac{\gamma_n\gamma_e T_2^e(\lambda M_z^n)(\lambda M_0^e)(\omega_0^e T_2^e)}{1+(\omega_0^e T_2^e)^2}M_{\perp}^n.\end{aligned} \tag{23}$$

Substituting Eq. (23) into Eq. (19), we find that the first term in Eq. (23) also influences the motion of nuclear spins. It is obvious that the in-phase component, that is, the term $\frac{\gamma_e\gamma_n T_2^e(\lambda M_z^n M_0^e)(\omega_0^e T_2^e)}{2\left[1+(\omega_0^e T_2^e)^2\right]}B_x$ of the induced magnetic field due to B_x decreases the total magnetic field, which is similar to Faraday's electronic-magnetic induction law. The in-quadrature component, that is, the term $i\frac{\gamma_e\gamma_n T_2^e(\lambda M_z^n M_0^e)}{2\left[1+(\omega_0^e T_2^e)^2\right]}B_x$ of the induced magnetic field due to B_x, leads to a frequency shift as follows:

$$\Delta\omega^n=-\frac{\gamma_e\gamma_n T_2^e(\lambda M_z^n M_0^e)}{2\left[1+(\omega_0^e T_2^e)^2\right]}B_x. \tag{24}$$

In the FID mode, the nuclear spins precess freely without B_x, and thus, we can use Eqs. (21) and (22) only. Otherwise, we should use Eqs. (21)–(24).

From Eq. (18), we find that when ω_0^e is larger, the induced magnetic field B_{in} is smaller. Thus, we could reduce the "radiation damping" effect in Rb-Xe comagnetometers through increasing B_0.

3. Numerical simulation and experiment

3.1. Numerical simulation

To assess the theoretical analysis, we can obtain numerical results using the coupled Eqs. (2) and (3). The parameters are the following: $B_0=0.5$ μT, $T_2^e=100$ μs, $T_2^n=20$ s, $\gamma_e=2\pi\times7000$ Hz/μT, $\gamma_n=2\pi\times10$ Hz/μT, $\lambda M_0^n=50$ nT, and $\lambda M_0^e=10$ nT. The initial parameters are $M_x^n=M_0^n/2, M_y^n=0, M_z^n=0$ and $M_x^e=M_y^e=0$, $M_z^e=M_0^e$. The numerical results are shown in Fig. 3(a), where the curve "damp" is M_x^n as a function of time t according to Eqs. (2) and (3), while the curve "no damp" is the expression for the free motion of nuclear spins, and we have $M_x^n=0.5M_0^e e^{-t/T_2^n}\cos(2\pi\times5.1t)$. It is evident that M_x^n relaxes faster due to the damping effect of Rb spins. Through exponential fitting, we obtain that the relaxation rate of the curve "damp" is 0.07 s^{-1}, which is adjacent to $\frac{1}{T_2^{n*}}=\frac{1}{T_2^n}+\frac{1}{T_{eq}^n}=0.05\ s^{-1}+0.0236\ s^{-1}=0.0736\ s^{-1}$.

The fast Fourier transform (FFT) of M_x^n in Fig. 3(a) is given in Fig. 3(b). The peak frequency of the curve "damp" is shifted by −5.5 mHz, which is smaller than that of the "no damp" curve. Thus, the precession frequency of nuclear spins is slowed due to the damping effect of electronic spins. The frequency shift is −8 mHz according to Eq. (22), which is larger than −5.5 mHz. Through careful checking, we found that M_z^n is changing with time in the FID process, and thus, the actual frequency shift is less than −8 mHz.

3.2. Experiment

It is difficult to verify the damping and frequency shift experimentally since we do not know the actual relaxation rate and precession frequency without electronic spins. However, from Eqs. (21) and (22), we find that the relaxation rate and frequency shift is dependent on B_0. Therefore, we can check the analysis through the variation in B_0.

The experimental apparatus is shown in Fig. 4. A spherical vapor cell with a diameter of 1 cm that contains an excess amount of ^{87}Rb metal, 2 Torr of ^{129}Xe and 300 Torr of N_2 is placed in an oven located inside a five-layer magnetic shield. The cell is heated with 200 kHz AC current flowing through a resistor film. A set of coils is used to produce the magnetic field B_0 in the z direction. The magnitude of B_0 is controlled by a current source and can be set in the range of 0–15 μT. The driving field B_x of 11.8 nT in magnitude is

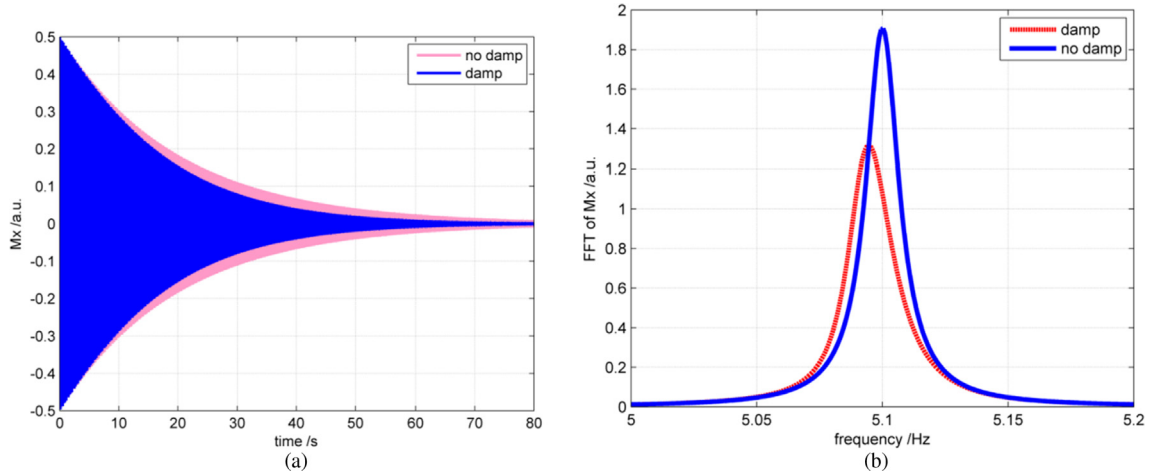

Fig. 3. (a) M_x^n as a function of time t and (b) the FFT of M_x^n.

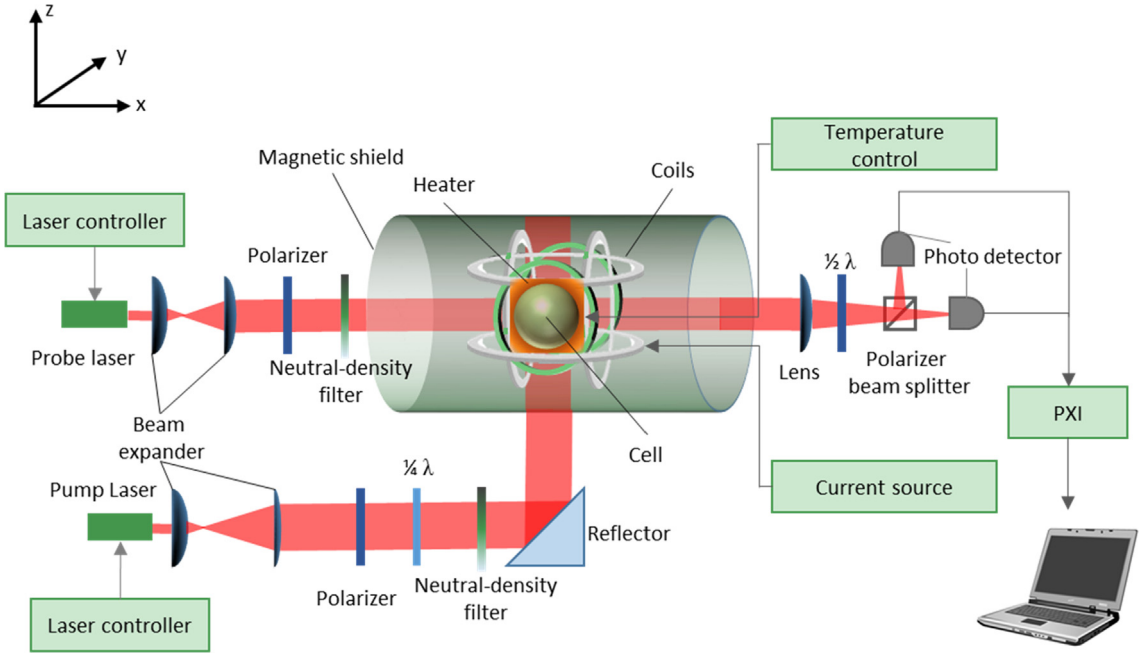

Fig. 4. Experimental setup.

produced by a data acquisition card and x coils. Both the pump laser and probe laser are expanded and aligned with the beam expander. The probe laser is 1 mW at the entrance of the magnetic field shield. The power of the pump laser can be tuned from 0 to 60 mW. With a polarizer and a 1/4 λ plate, the polarization of the pump laser is set to be circularly polarized. After reflection by the triangle reflector, the pump laser propagates along the z direction and pumps the Rb atoms. With a linear polarizer, the polarization of the probe laser is set to be linearly polarized. The intensity of both the pump and probe laser can be adjusted by the neutral-density filter. After propagating through the cell, the polarization of the probe laser is detected with polarimetry consisting of a lens, a polarization beam splitter and two photo detectors. The measurement process is controlled by a Labview program.

In the experiment, we change B_0 through tuning the current source. At each B_0, we measure the magnetic resonance frequency and transverse relaxation time of Xe spins by the free induction decay method. We conducted the experiment under two conditions with different temperatures and pump powers.

Case 1: The temperature of the heater is stabilized at 85 °C and the power of the pump laser is set to be 10 mW at the entrance of the magnetic field shield.
Case 2: The temperature of the heater is stabilized at 95 °C and the power of the pump laser is set to be 40 mW at the entrance of the magnetic field shield.

At first, we measure the following quantities: T_2^e, λM_0^n, and λM_0^e. Through scanning the magnetic resonance curve of Rb atoms, the bandwidth of magnetic resonance Δf can be obtained. The transverse relaxation time of Rb atoms is $T_2^e = 1/(\pi\Delta f)$. Through calibration with a specific magnetic field along the x-axis, the scale factor of the Rb magnetometer k_{Rb} can be obtained. With a $\pi/2$ pulse on the nuclear spins, we can obtain the value of λM_0^n. Through flipping the polarization of the pump laser from left to right circularly polarized [20,21], we can obtain the value of λM_0^e. These parameters for case 1 and case 2 are given in Table 1. The gyromagnetic ratios are $\gamma_n = 2\pi \times 11.87$ Hz/μT and $\gamma_e = 2\pi \times 7000$ Hz/μT for ^{129}Xe and ^{87}Rb, respectively. Therefore, we can theoretically obtain

Table 1
Measured parameters.

	T_2^e/μs	λM_0^n/nT	λM_0^e/nT
Case 1	31.8	16.6	3.5
Case 2	15.9	35.0	9.0

the relaxation rate and frequency shift for Xe spins caused by the back action of Rb spins.

The measured relaxation rate Γ_m can be expressed as

$$\Gamma_m = \frac{1}{T_2^{n*}} = \frac{1}{T_2^n} + \frac{1}{T_{eq}^n} = \frac{1}{T_2^n} + \frac{\gamma_n\gamma_e T_2^e(\lambda M_z^n)(\lambda M_0^e)}{1+(\gamma_e T_2^e B_0)^2}, \tag{25}$$

where the first term is independent of the "radiation damping" and the second term results from the "radiation damping".

The measured magnetic resonance frequency of Xe spins f_m can be expressed as follows:

$$f_m = \frac{1}{2\pi}\left(\gamma_n B_0 + \frac{1}{2}\frac{\gamma_n B_{\perp 0}^2}{B_0} - \gamma_n\gamma_e T_2^e(\lambda M_z^n)(\lambda M_0^e)\frac{(\gamma_e T_2^e B_0)}{1+(\gamma_e T_2^e B_0)^2}\right), \tag{26}$$

where $B_{\perp 0}$ is the possible residual magnetic field in the xy plane and the three terms result from B_0, $B_{\perp 0}$ and "radiation damping".

To verify Eqs. (25) and (26) experimentally, we change B_0 and measure the relaxation rate Γ_m and magnetic resonance frequency f_m at each B_0. We fit the experimental data for Γ_m as a function of B_0 by equation $\Gamma_m = a_0 + \frac{a_1}{1+a_2 B_0^2}$ so that the relaxation rate caused by "radiation damping" and $T_2^e = \sqrt{a_2}/\gamma_e$ can be obtained. Afterwards, we use equation $f_m = b_0 + b_1 B_0 + \frac{b_2}{B_0} - \frac{b_3 B_0}{1+a_2 B_0^2}$ to fit the experimental data for f_m as a function of B_0 so that the frequency shift due to "radiation damping" can be distinguished. The fitting parameters we obtained are listed in Table 2. The values of the relaxation rate $\frac{a_1}{1+a_2 B_0^2}$ and frequency shift $-\frac{b_3}{1+a_2 B_0^2}$ are given in Figs. 5 and 6, which are denoted as "exp.". At the same time, the theoretical results using Eqs. (21) and (22) and data in Table 1 are also given and are denoted as "theory" in the legend. It is evident that

Table 2
Fitting parameters.

	a_0	a_1	a_2	b_0	b_1	b_2	b_3
Case 1	0.023	0.006	4.6	−0.003	11.87	0.0005	0.0015
Case 2	0.051	0.013	0.66	0.0924	11.87	0.0005	0.0056

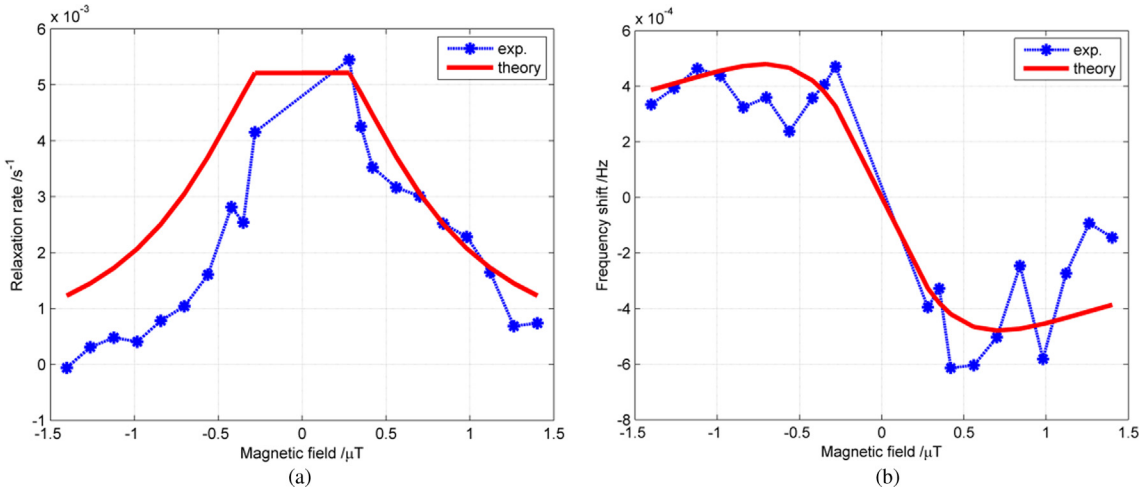

Fig. 5. Relaxation rate (a) and frequency shift (b) as a function of B_0 for case 1.

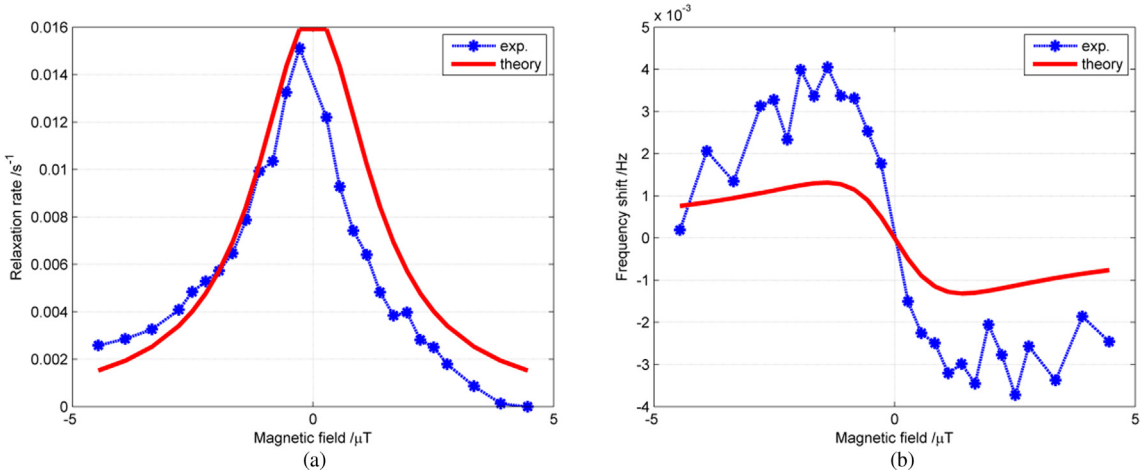

Fig. 6. Relaxation rate (a) and frequency shift (b) as a function of B_0 for case 2.

the experimental results agree well with the theoretical results for case 1 in spite of a little drift of the experimental parameters in the measurement process. However, the experimental results have slightly larger disagreement with the theoretical results for case 2, especially on the frequency shift curve. The experimental frequency shift is larger than the theoretical value in the range of −4 to 4 μT. The reason for this might be when the polarization of Rb spins is higher, the perturbation-iteration method has larger error. From Eqs. (25) and (26), we know that b_3 should be equal to $\frac{1}{2\pi}a_1\sqrt{a_2}$. In case 1, we have $\frac{1}{2\pi}a_1\sqrt{a_2} = 0.0020$, which is very close to 0.0015. In case 2, however, we have $\frac{1}{2\pi}a_1\sqrt{a_2} = 0.0017$, which is much smaller than 0.0056. Thus, the error in case 2 is larger. This phenomenon needs to be studied further.

3.3. Discussion

A NMR signal is conventionally detected via a resonant coil, where the coil has back action on the NMR system, thereby causing damping and a frequency shift. In the spin-exchange optically pumped NMR systems, the NMR signal is detected by the magnetometer consisting of electronic spins and a probe laser. The back action of the magnetometer is similar to the detection coils, which also leads to damping and a frequency shift. Even there is no radiation field, the polarized electronic spins produce a virtual radiation field out of phase. As a result, the precession is damped. We might as well call this effect the "radiation damping" effect.

We would like to discuss the damping and frequency shift effects in an NMR probe, which detects fundamental physical constants operating in an FID mode. A typical example is given in [3], where the frequency stability is vital to the measurement. According to the experimental parameters given in [3,21,22], we could estimate some specific values. For the Rb-Xe system, the enhancement factor is $\kappa_0 \approx 493$ and $\lambda = 2\kappa_0\mu_0/3$. The ^{129}Xe precesses with a frequency of 152 Hz so that the static magnetic field in the z direction is approximately 12 μT. The cell is heated to 130 °C, and the Rb density is approximately $10^{13}/\text{cm}^3$. The T_2^e is 25 μs, and

the Rb atoms are polarized to 50%. We assume that the ^{129}Xe is 5 Torr and polarized to 10%. According to Eqs. (21) and (22), we can obtain the following:

$$\frac{1}{T_{eq}^{n}} = 2.4 \times 10^{-5}\mathrm{s}^{-1} \tag{27}$$

and

$$\Delta\omega^{n} = 2\pi \times 50\ \mu\mathrm{Hz}. \tag{28}$$

Under such conditions, the frequency shift due to the "radiation damping" effect is not negligible.

From Eqs. (21) and (22), we know the larger the ω_0^e is, the smaller the effects of damping and the frequency shift. This is because when ω_0^e is large, the sensitivity of the Rb magnetometer to the low frequency magnetic field is reduced, which gives a low signal-to-noise ratio (SNR). This means if the sensitivity of the magnetometer is improved, the electronic spins strongly quicken the relaxation. It can be easily understood in a physical view since high sensitivity means strong interaction and therefore leads to strong relaxation.

In the FID mode, M_z^n will change from zero to M_0^n exponentially; therefore, both T_{eq}^n and $\Delta\omega^n$ will change remarkably. For a dual species NMR oscillator operating in the FID mode, due to different γ_n and M_0^n, the frequency shifts are different and cannot be effectively common-mode suppressed. This will decrease the accuracy of the measurement. In Ref. [3], the magnetic field from polarized Rb atoms is approximately 10 nT, leading to a frequency shift of 0.12 Hz for ^{129}Xe. After common-mode suppression with the dual species nuclear magnetic resonance method, the residual frequency shift is approximately 204 μHz. This error currently limits the precision of NMR oscillators. The frequency shift due to the "radiation damping" is on the order of 10 μHz and may be the largest error after the error caused by polarized Rb atoms is further reduced. The "radiation damping" may also be an error source for the magnetometer using Xe nuclear spins, such as in [22].

"Radiation damping" also has an effect on the measurement of the relaxation time. In the FID mode, the relaxation time we obtain includes the effect of "radiation damping", which is smaller than the actual relaxation time. In lower B_0, the magnetic gradient caused by B_0 is small, but the "radiation damping" effect is strong. Meanwhile, in higher B_0, the magnetic gradient caused by B_0 is large. In some experiments such as testing the fifth force or surface relaxation measurements, the relaxation time is used as a probe. The "radiation damping" may cause error to some extent.

Some NMR oscillators work in a continuous mode, for example, NMR gyros [23]. To sustain the oscillation, the driving magnetic field is applied in the x-axis direction. According to Eqs. (23) and (24), this driving magnetic field will decrease the precession frequency. The frequency shift is proportional to Bx; therefore, the oscillation frequency of the oscillators will be affected by the amplitude of Bx. This error is difficult to suppress with the dual species method since the frequency shifts are uncorrelated. Moreover, the "radiation damping" depends on T_2^e, M_0^e and M_z^n, and the precession frequency can be shifted due to polarization fluctuations of electronic spins.

4. Conclusion

In the comagnetometers, interactions between spin ensembles through magnetization act as "radiation damping", which leads to damping and a frequency shift of the rotating spin ensembles. In the FID mode, since the rotating magnitude varies with time, the equivalent relaxation time and frequency shift will also change with time. In the self-oscillation mode, the equivalent relaxation time and frequency shift may change with polarization fluctuations and variation of external excitation fields. Therefore, these effects should be taken into account to improve the accuracy of NMR probes for new physics. To reduce the "radiation damping" effect, we can use a larger static magnetic field for those comagnetometers using the precessing frequency to detect physical parameters.

Acknowledgments

This work was supported by the Research Project of the National University of Defense Technology (grant number ZK18-02-04), the Natural Science Foundation of China (grant numbers 61671458, 61571018, 61571003, and 91436210), and the Natural Science Foundation of Hunan Province (grant number 2018JJ3608).

References

[1] F. Allmendinger, W. Heil, S. Karpuk, W. Kilian, A. Scharth, U. Schmidt, A. Schnabel, Yu. Sobolev, K. Tullney, New limit on Lorentz-invariance- and CPT-violating neutron spin interactions using a free-spin-precession ^{3}He-^{129}Xe comagnetometer, Phys. Rev. Lett. 112 (2014) 110801.
[2] V.A. Kostelecký, C.D. Lane, Constraints on Lorentz violation from clock-comparison experiments, Phys. Rev. D 60 (1999) 116010.
[3] M. Bulatowicz, R. Griffith, M. Larsen, J. Mirijanian, C.B. Fu, E. Smith, W.M. Snow, H. Yan, T.G. Walker, Laboratory search for a long-range T-Odd, P-Odd interaction from axionlike particles using dual-species nuclear magnetic resonance with polarized ^{129}Xe and ^{131}Xe gas, Phys. Rev. Lett. 111 (2013) 102001.
[4] W. Zheng, H. Gao, B. Lalremruata, Y. Zhang, G. Laskaris, W.M. Snow, C.B. Fu, Search for spin-dependent short-range force between nucleons using optically polarized ^{3}He gas, Phys. Rev. D 85 (2012) 031505(R).
[5] A.K. Petukhov, G. Pignol, D. Jullien, K.H. Andersen, Polarized ^{3}He as a probe for short-range spin-dependent interactions, Phys. Rev. Lett. 105 (2010) 170401.
[6] C.B. Fu, T.R. Gentile, W.M. Snow, Limits on possible new nucleon monopole-dipole interactions from the spin relaxation rate of polarized ^{3}He gas, Phys. Rev. D 83 (2011) 031504(R).
[7] A.P. Serebrov, New constraints for CP-violating forces between nucleons in the range 1 micrometer to 1 centimeter, Phys. Rev. B 680 (2009) 423–427.
[8] H. Yan, W.M. Snow, New limit on possible long-range parity-odd interactions of the neutron from neutron-spin rotation in liquid ^{4}He, Phys. Rev. Lett. 110 (2013) 082003.
[9] G. Vasilakis, J.M. Brown, T.W. Kornack, M.V. Romalis, Limits on new long range nuclear spin-dependent forces set with a K-^{3}He comagnetometer, Phys. Rev. Lett. 103 (2009) 261801.
[10] T.W. Kornack, M.V. Romalis, Dynamics of two overlapping spin ensembles interacting by spin exchange, Phys. Rev. Lett. 89 (2002) 253002.
[11] Z.G. Wang, X. Peng, H. Luo, H. Guo, Comparison of operation modes for spin-exchange optically-pumped spin oscillators, J. Magn. Reson. 278 (2017) 134–140.
[12] D. Sheng, A. Kabcenell, M.V. Romalis, New classes of systematic effects in gas spin comagnetometers, Phys. Rev. Lett. 113 (2014) 163002.
[13] T.E. Chupp, R.J. Hoare, R.L. Walsworth, B. Wu, Spin-exchange-pumped ^{3}He and ^{129}Xe Zeeman masers, Phys. Rev. Lett. 72 (1994) 2363–2366.
[14] C.R. Bruce, R.E. Norberg, G.E. Pake, Radiation damping and resonance shapes in high resolution nuclear magnetic resonance, Phys. Rev. 104 (1956) 419–420.
[15] N. Bloembergen, R.V. Pound, Radiation damping in magnetic resonance experiments, Phys. Rev. 95 (1954) 8–12.
[16] V.V. Krishnan, N. Murali, Radiation damping in modern NMR experiments: progress and challenges, Prog. Nucl. Mag. Res. Sp. 68 (2013) 41–57.
[17] E.J. Eklund, Microgyroscope Based on Spin-Polarized Nuclei, University of California, Irvine, 2008, pp. 30–50.
[18] T.G. Walker, W. Happer, Spin-exchange optical pumping of noble-gas nuclei, Rev. Mod. Phys. 69 (2) (1997) 629–642.
[19] T.W. Kornack, R.K. Ghosh, M.V. Romalis, Nuclear spin gyroscope based on an atomic co-magnetometer, Phys. Rev. Lett. 95 (2005) 230801.
[20] S.R. Schaefer, G.D. Cates, T.R. Chien, D. Gonatas, W. Happer, Frequency shifts of the magnetic-resonance spectrum of mixtures of nuclear spin-polarized noble gases and vapors of spin-polarized alkali-metal atoms, Phys. Rev. A 39 (11) (1989) 5613–5623.
[21] Z.L. Ma, E.G. Sorte, B. Saam, Collisional ^{3}He and ^{129}Xe frequency shifts in Rb–noble-gas mixtures, Phys. Rev. Lett. 106 (2011) 193005.
[22] M. Bulatowicz, M. Larsen, Compact atomic magnetometer for global navigation (NAV-CAM), Posit. Locat. Navig. Symp. 82 (2) (2012) 1088–1093.
[23] T.G. Walker, M.S. Larsen, Spin-exchange-pumped NMR gyros, Adv. Atom. Mol. Opt. Phys. 65 (2016) 373–401.